Article:
Vafaei, S and Wen, D (2014) Critical heat flux of nanofluids inside a single microchannel: Experiments and correlations. Chemical Engineering Research and Design, 92 (11). pp. 2339-2351. ISSN 0263-8762

https://doi.org/10.1016/j.cherd.2014.02.014

Critical Heat Flux of Nanofluids inside a Single Microchannel: Experiments and Correlations

Saeid Vafaei[1*] and Dongsheng Wen[2]

[1]Department of Mechanical, Materials and Manufacturing, EPSRC Centre for Innovative Manufacturing in Additive Manufacturing, University of Nottingham, Nottingham, UK.

Email: Saeid.Vafaei@nottingham.ac.uk

[2]School of Process, Environmental and Materials Science, University of Leeds, Leeds, UK.

Email: d.wen@leeds.ac.uk

Abstract: This study investigated experimentally the flow boiling CHF phenomena of aqueous-based alumina nanofluids in single microchannels, and assessed the validity of a number of microchannel-based CHF correlations using experimental nanofluids data. While the usual approaches for CHF enhancement are through the modification of different tube surfaces or employing different inserts, this work showed that CHF in microchannels can be enhanced significantly by the inclusion of small concentrations of nanoparticles. The CHF value is found to increase with the increase of mass flux, initial subcooling and alumina nanoparticle concentrations. The maximum subcooled CHF enhancement occurred at the lowest mass flux and highest alumina concentration within the experimental range. In addition, the Lee and Mudawar correlation is modified to predict the critical heat flux of water and nanofluids. The new model is examined by experimental data and 24% and 30% mean absolute error are observed for water and alumina nanofluid respectively.

Keywords: Nanofluids, Nanoparticle, Microchannel, Flow boiling, Critical heat flux, Empirical correlations.

1. Introduction

For cooling systems based on phase change mechanism, the safe operation of the system is limited by the critical heat flux (CHF), which is the upper limit of heat removal without incurring serious surface temperature jump. Beyond that, a vapor blanket or local dryout will occur on the heated surface that prevents further direct contact with liquid, which would result in rapid rise in the surface temperature that might bring a catastrophic

effect to the whole system. For safety considerations, significant effort has been spent in the last to understand the influential factors and the mechanisms of CHF in conventional-sized channels [Lee and Mudawar 2009; Roday et al 2008; Roday and Jensen 2009b,c]. Conventional approaches of increasing CHF include engineering different tube surfaces (grooved tubes or structured modified surfaces), employing different inserts (such as twisted tape or helically coiled wire) in tubes, or applying an external field to induce fluid vibrations.

With the rapid progress of micro/nanotechnologies, a number of small integrated functional devices, such as the micro/nano electronic-mechanical systems (MEMS /NEMS), lap-on-a-chip devices and high-heat flux laser systems, have been developed. Due to the increasing importance of surface forces and evaporative momentum at small dimensions, many differences have been found on the mechanisms of CHF between large and small channels [Lee and Mudawar 2009; Roday et al 2008]. There is an increasing effort to understand the mechanisms of CHF in microchannels and develop reliable models correspondently. In the last decade, there was intensive effort, worldwide in using nanoparticle suspensions, or so called nanofluids, to modify thermo physical properties of heat transfer fluids and intensify different heat transfer processes. Quite a few studies have shown that dilute nanofluids can significantly increase the CHF under pool boiling conditions [Bang and Chang 2005; Kim et al 2007c]. Very recently, a few limited studies have been extended to flow boiling conditions. For instance, Kim et al (2008) studied nanofluid flow boiling in a conventional-sized stainless steel tube ($d = 8.7\text{mm}$), and reported that the CHF increased 30% under a 0.01v% alumina nanoparticle concentration. Vafaei and Wen (2010a) investigated subcooled CHF of aqueous alumina nanofluid in 510 μm single microchannels, and reported an increase of ~51 % in CHF at a nanoparticle concentration of 0.1 v%.

Concerning the emergence of both nanofluids and microchannels, the focus of this study is two folds: i) to extend the spectrum of our knowledge in nanofluids by experimentally investigating the CHF phenomenon of aqueous-based alumina nanofluid in single microchannels, and ii) to assess the existing correlations' and applicability on nanofluids data. In this paper, a short review of CHF in microchannels and CHF with nanofluids will be conducted. It will be followed by an experimental study of the CHF

phenomenon of nanofluids in single microchannels; an assessment of the applicability of different existing CHF correlations. In addition, a correlation based on the Lee and Mudawar model is modified to predict the critical heat flux of water and nanofluid in microchannels, using existing experimental data.

2. Critical Heat Flux in Microchannels

Even though, the critical heat flux phenomenon has been studied for a long time on macroscale sizes, the transition into the microscale study is still at the beginning. A number of studies have been conducted to investigate the influence of various parameters on the CHF, propose different correlations and/or mechanisms. Generally the critical heat flux in microchannels has been found to be affected by the channel geometries (size, shape and heated length) and operational conditions (mass flux, exit vapor quality, inlet subcooling and pressures), as well as a few other parameters, which are summarized in Table 1. Many inconsistent results have been reported in the literature, including different CHF trends as the channel becomes smaller, i.e some studies reported an increase in CHF in smaller channels [Lee and Mudawar 2009; Roday et al 2008; Roday and Jensen 2009b] while others reported a totally different trend [Mudawar and Bowers 1999]. A brief review of existing critical heat flux is given below.

Some early studies revealed a qualitative trend of CHF in mini or microchannels. Lazarek and Black (1982) showed that for saturated flow boiling of R-113 inside a stainless steel tube, the CHF is occurred toward the exit of heated channel; a correlation was developed to predict the local quality for the onset of saturated critical heat flux. Inasaka and Nariai (1987) investigated the subcooled critical heat flux and void fraction of water inside stainless steel tubes of various size ($d = 1 - 3mm$) and found that CHF increased inside narrower tubes for a given mass flux. Vandervort et al (1994) investigated subcooled CHF inside metallic tubes made of stainless steel, nickel, brass and inconel in the range of 0.3-2.7 mm diameters. The CHF value was found to be insensitive to the tube materials; CHF was smaller at a higher heated length to diameter ratio, especially when L/D became smaller than 10.

Lee and Mudawar (2009) measured subcooled CHF of HFE 7100 in a three-side heating copper microchannel with simultaneous visualization through a high-speed video. The increase in inlet subcooling was found to enhance CHF significantly because a high

subcooling reduced both bubble departure diameter and void fraction, limiting the flow pattern in the bubbly regime. Similar results were obtained by Mudawar and Bowers (1999) for subcooled flow boiling of water in small stainless steel tubes at high mass velocities, which showed that CHF increased nearly linear with the increase of subcooling. For saturated CHF, Qu and Mudawar (2004) studied water flow boiling inside a copper microchannel heat sink containing 21 parallel 0.215 × 0.821 mm channels, and observed a strong vapor reverse flow phenomenon, which re-mixing with inlet flow; cancelled the effect of inlet subcooling. Consequently the critical heat flux became insensitive to the inlet temperature. Similarly, Bowers and Mudawar (1994) showed that for an oxygen-free copper multichannel (0.510 by 2.54 mm), the CHF inside minichannels and microchannels is independent of the inlet subcooling at low flow rates, because the working fluid reached to the saturation temperature at a short distance inside the heated channel. Wojtan et al (2006) investigated the saturated CHF inside single stainless steel tubes of 0.5 mm and 0.8 mm for two refrigerants: R-134a and R-245fa. It was observed that CHF increased with increasing mass flux. The critical heat flux inside 0.8 mm microchannel was higher than of 0.5 mm one for a given mass flux and the difference became larger as the mass velocity increased. It was reported that the highest CHF occurred at the shortest heated length and highest mass flux. Negligible influence of liquid subcooling in range of 2-15 ^{o}C was also noticed. Agostini et al (2008) conducted a saturated CHF measurement of R-236fa inside 67 parallel silicon-based channels in the size of 223 × 680 μm . The effect of inlet saturation temperatures ($20.31 \le T_{sat,i} \le 34.27^{o}C$) and the inlet subcoolings ($0.4 \le \Delta T_{sub,i} \le 15.3^{o}C$) were found negligible on the saturated CHF value. A theoretical model was proposed to predict the saturated critical heat flux in circular microchannels [Revellin and Thome 2008]. The dryout process of a liquid film in annular flow was modeled by solving the one-dimensional two-phase flow conservation equations numerically. It was assumed in the model that interfacial waves, usually observed in microchannel annular flows, would trigger an early onset of dryout when the film thickness was smaller than the height of the interfacial wave.

In addition, Kuan and Kandlikar (2008) experimentally studied the critical heat flux of water and R-123 inside six parallel channels ($1054 \times 157\ \mu m$). The effects of flow instabilities in microchannels were investigated using flow restrictors at the inlet of each channel to stabilize the flow boiling process and avoid the backflow phenomenon. It was found that the critical heat flux increased with increasing Weber number. Roday et al (2008) & Roday and Jensen (2009) conducted CHF experiments of water in a uniformly heated single micro tube under both subcooled and saturated conditions. They employed a needle valve to provide a large pressure drop upstream of the test section, specifically to avoid instabilities. Under similar mass flux, heated length to diameter ratio and exit pressure conditions, the CHF was found to be increased substantially with the reduction of tube diameter from 0.427 mm to 0.286 mm. However, the difference was small for tubes with diameters of 0.7 mm and 0.427 mm. Other observations showed that CHF decreased with the increase of heated length for 0.286 mm and 0.7 mm tubes and increased with the increase of mass flux and exit pressure. Under subcooled conditions, CHF exhibited a decreasing trend with the increase of exit quality, but a reverse trend was observed for saturated boiling. Kosar and Peles (2007) studied the effect of mass flux, exit quality, and exit pressure on saturated CHF of R-123 inside five parallel silicon-based channels of $200 \times 264\ \mu m$ and $1\ cm$ length. The critical heat flux was triggered at relatively high qualities during the annular flow. The visualization of flow pattern and relatively high exit quality at the CHF condition suggested that critical heat flux was a result of local dryout. Parallel studies were conducted for water [Kosar et al 2005], and similarly, it was found that the boiling number at the critical heat flux condition was approximately a constant [Kuo and Peles 2008]. Qi et al (2007a,b) measured the saturated critical heat flux of liquid nitrogen in tubes with diameters of 0.531, 0.834, 1.042 and 1.931 mm, and realized CHF increased as the channel diameter decreased under given conditions. Park and Thome (2010) measured the saturated critical heat flux inside 20 parallel ($467 \times 4052\ \mu m$), and 29 parallel ($199 \times 756\ \mu m$) copper channels for R-134a, R-236fa, and R-245fa. It was shown that as channel size decreased the effect of inlet subcooling played a smaller role.

The above short review showed that many inconsistent results were reported, yet our present understanding of CHF in microchannels is limited. These discrepancies might

have roots in different experimental conditions and affected by different properties of working fluids. For the influence of channel size, Doroshckuk et al (1975) proposed a correction factor for the channel diameter as

$$\frac{q_{m,d_i}}{q_{m,d_i=8mm}} = \left(\frac{d}{8}\right)^n \tag{1}$$

$n = -0.5$ was suggested for channel diameter between 4 and 16 mm. For smaller channels, the channel dimension was incorporated in different correlations. Different trends of channel size influence can be reflected from different correlations.

3. Critical Heat Flux of Nanofluids

The study of nanofluids [Wen et al 2009] started over a decade ago aiming to enhance the thermo physical properties of different heat transfer fluids [Buongiorno et al 2009], with late applications in single phase forced convection heat transfer [Wen and Ding 2004; Rea et al 2009] and two-phase convective (pool boiling, flow boiling and in-tube condensation) heat transfer. It has been generally observed the presence of nanoparticles inside a base liquid increased the critical heat flux for pool boiling [Bang and Chang 2005; Kim et al 2007c] and flow boiling in macroscale channels [Kim et al 2008;, Kim et al 2009] and microchannels [Rea et al 2009]. However the quantitative results still differ: the CHF enhancement has been reported to vary from 10-40% [Bang and Chang 2005] to 200-400% [Kim et al 2007c]. It is difficult to explain such wide differences. The possible reasons reside in the stability of nanofluids and the variability of the solid and the liquid phases, as well as the surface wettability change due to complicated interactions between nanoparticles and the heating surface. Most of nanofluids used in boiling experiments tend to be unstable at the high temperatures due to the failure of stabilizers. The stabilizers and particles could agglomerate and deposit on the heating surface, which certainly modifies the heating surface and brings about a number of unforeseen effects, including the change of active nucleate cavities, the modification of surface wettability and the formation of extra thermal resistance on the heating surface that prevents direct contact of liquid with the boiling surface [Wen 2008a,b]

Apart from the stability issue, the inherent interactions of nanoparticles with the heating surface, which may result in particle deposition and surface wettability change, is

believed to be responsible for many different observations. It has been shown that the concentration of nanoparticles inside liquid microlayer beneath the bubble could increase as a result of the evaporation and nanoparticle deposition, forming a tiny porous layer of nanoparticles. The deposited layer of nanoparticles modifies the surface wettability of heating surface and consequently increases the critical heat flux [Kim et al 2007c; Kim et al 2008; Kim et al 2009]. The thickness of the porous layer may increase with the increase of nanoparticle concentrations [Bang and Chang 2005; Vafaei and Wen 2010a]. It was also observed that the use of nanofluids mitigated the propagation of hot spots that could explain why burnout tends to be more localized compared to water [Kim et al 2008], which might be caused by an increased surface wettability as a result of the particle deposition [Kim et al 2009]. A variety of reasons can contribute to the wettability change, which include the deposition of nanoparticles upon heating [Bang and Chang 2005; Kim et al 2007b,c], the modification of force balance at the triple line [Vafaei et al 2006; Vafaei and Podowski 2005; Vafaei and Podowski 2004], and the changes in the gas-liquid [Vafaei et al 2009] and solid surface tensions [Vafaei and Podowski 2005, Vafaei et al 2010] by suspended nanoparticles. The behavior of triple line has a significant effect dynamics of bubble growth, and bubble departure [Vafaei and Wen 2010b,c,d,e; Vafaei et al 2011a,b; Vafaei and Wen 2011a], which will affect the occurrence of the critical heat flux.

The tiny layer of deposited nanoparticles would change the surface roughness and wettability. For the given conditions, modification of surface wettability has reported to be more significant, compared to the variation of surface roughness [Kim et al 2009]. Initially, the enhancement of wettability due to the tiny layer of deposited nanoparticle [Kim et al 2009; Kim et al 2007a; Gerardi et al 2010] was reported to be a possible reason for enhancement of critical heat flux for nanofluids and effects of surface wettability on critical heat flux has considered theoretically by the macrolayer dryout model [Haramura and Katto 1983] and the hot/dry spot theory [Theofanous and Dinh 2006]. But later on, further experiments have conducted and indicated that all of the hydrophobic, hydrophilic, and superhydrophilic surfaces enhance the pool boiling critical heat flux [Forrest et al 2010]. Since the pool boiling critical heat flux was enhanced by

both hydrophobic and hydrophilic surfaces, the surface wettability might not be the only possible reason for the critical heat flux enhancement.

The receding contact angle occurs in boiling heat transfer when the triple line moves toward the liquid phase while the advancing contact angle manifests when the contact line moves toward the gas phase [Mukherjee and Kandlikar 2007]. The difference between receding and advancing contact angle is called contact angle hysteresis. The suspended and deposited nanoparticles are able to change the receding and advancing contact angles as well as the equilibrium contact angle [Vafaei et al 2006]. The effect of the receding contact angle on critical heat flux was modeled theoretically [Kandlikar 2001; Kandlikar and Steinke 2002]. Experimental results verified that surfaces with low receding contact angles were observed to enhance the critical heat flux [Forrest et al 2010]. The equilibrium, advancing and receding contact angles of the (20 Bilayers PAH/ SiO_2, calcinated, fluorosilane) hydrophobic heated surface respectively were 140^o, 160^o, and 20^o [Forrest et al 2010]. This surface was found to simultaneously enhance the boiling heat transfer coefficient and critical heat flux. Roughness and non homogeneity of working fluids and surface are parameters affecting the hysteresis, receding, and advancing contact angles. Further investigations are required to find out the relation between surface roughness, wettability, receding and advancing contact angles and eventually the reasons for the enhancement of the critical heat flux and boiling heat transfer coefficient. It is essential to find the particular conditions that enhance the boiling heat transfer coefficient and the critical heat flux of nanofluids simultaneously.

4. Existing correlations for flow boiling critical heat flux

A number of correlations have been proposed to predict CHF under subcooled conditions. For instance, Tong (1968) proposed a subcooled critical heat flux correlation for high operational pressure of 7-14 MPa based on the boundary layer separation model. Subsequently, Inasaka and Nariai (1987) modified the Tong model by changing its coefficient, C. The new coefficient of C was pressure dependent and decreased with the increase of system pressure. Following a similar concept, Celata et al (1993, 1994) also modified the Tong model to raise the accuracy of prediction of critical heat flux in the range of pressures below 8.4 MPa by adjusting the coefficient C and exponential power of the Reynolds number.

Hall and Mudawar (2000a,b) conducted a parametric study on critical heat flux of subcooled water in small tubes and found that the CHF is inversely proportional to the tube diameter. Their correlations were examined by an extensive database (5544 data points) to obtain best possible coefficients with the least possible prediction error. The correlation predicted the subcooled critical heat flux with a mean absolute error of 10.3% and root mean square errors of 14.3%. The subcooled CHF correlated by Hall and Mudawar (1999) reached a mean absolute error of 17%-24%. Similarly the Vandervort et al. model (1994) predicted the subcooled critical heat flux with a root mean square deviation of 10%. Lee and Mudawar (2009) developed a systematic technique to modify the existing subcooling CHF correlations inside microchannels, which were examined by given experimental data for different hydraulic diameters, mass fluxes and inlet subcoolings. The Lee and Mudawar model (2009) predicted the critical heat flux with a mean absolute error of 8 % and all the data falling within ±20% of the predictions.

Assessed by obtained subcooled CHF data, Roday and Jensen (2009a) proposed a correlation of critical heat flux for subcooled flow boiling based on the inlet conditions and four non-dimensional variables, i.e. Weber number (based on tube inside diameter), the density ratio, heated length-to-diameter ratio and the enthalpy or inlet quality. For a given experimental data, the correlation predicted the Boiling number with a root mean square error of 34.3 % and mean absolute error of 26.3 %.

Similar to subcooled critical heat flux, many correlations have been developed to predict the saturated critical heat flux in macroscales as well as microscales. These correlations are generally valid only within the range of their experimental data, and should be cautious to be extended to different conditions. Katto (1978) developed critical heat flux correlations for different regimes: H-regime where the CHF was affected by the hydrodynamic instability, L-regime when the mass flux was smaller than that in H-regime, and HP-regime that occurred when the pressure effect was significant. The Katto model was modified for the saturated critical heat flux, i.e the Katto and Ohno model (1984), where the subcooling condition was taken into account. Qu and Mudawar (2004) introduced a new correlation based on the Katto-Ohno model and assessed it with the critical heat flux data of water in rectangular microchannels and R-113 in circular mini/microchannels given by Bowers and Mudawar (1994). The overall mean absolute

error of 4% was observed for both water and R-113. The correlation proposed by Bowers and Mudawar (1994) has been shown good agreement with experimental data for mini/microchannels. Wojtan et al (2006) also modified the Katto-Ohno model into a simpler correlation to predict the saturated critical heat flux based on their experimental data in single, circular, uniformly heated microchannels. The model achieved a mean absolute error of 7.6 %, and 82.4% of data falling within a ± 15 % error bounds. Qi et al (2007a) developed a correlation based on the Katto correlation to predict the critical heat flux of liquid nitrogen in channels of size $0.531 \prec d_i\,(\text{mm}) \prec 1.931$, which achieved a mean absolute error of 7.38%.

In addition, Zhang et al (2006) developed a new correlation for flow boiling of water in small-diameter tubes ($0.33 \prec d_h\,(\text{mm}) \prec 6.22$) based on a database of 2539 points, and achieved an overall mean deviation of 16.8 %. Kosar and Peles (2007) developed a correlation to include the pressure effect inside a multichannel ($200 \times 264\ \mu\text{m}$) for R-123. The correlation predicted the saturated CHF with a mean absolute error of 3.8% for R-123. Similar correlation developed for water achieved a mean absolute error of 7.4% (2005). Kuan and Kandlikar (2008) developed a new correlation, by employing force balance along the channel and considering forces due to inertia, momentum change and surface tension. The model predicted the critical heat flux with mean absolute error of 16.4% and 8.2% respectively for given experimental data of R-123 and water, when the value of constant C was set as 0.002679.

5. Experimental Setup

An open loop microchannel experimental system, shown in Figure 1, is built to conduct critical heat flux measurement of water and aqueous alumina nanofluid. The system includes a syringe pump, a stainless steel microchannel, a heating and insulation unit, a storage tank and a data acquisition (DAQ) system for power, pressure and temperature measurement. The sampling rate of all data measurement is 1 kHz. The microchannel is made from stainless steel with 160 μm wall thickness, internal diameter of 510 μm, and length of 306 mm. The microchannel was insulated by a thick layer of Armaflex and rock wool insulator, and heated electrically through a variable DC power source, which provided uniform heat flux over the test section. Calibrated K-type

thermocouples with a tip diameter of 0.08 mm diameter were installed along the surface of the microchannel to obtain the surface temperature distribution along the tube. Two thermocouples were used to measure the inlet and outlet fluid temperature. Two cross unions were connected at the inlet and outlet of the microchannel to supply the liquid passage, and spaces for temperature and pressure sensors. Pressure sensors were four-active piezoresistive bridge devices in the range of 0-100 psi. Simultaneous temperature and pressure signals were recorded by the DAQ system through controlled by a Labview program. A low pass filter was installed to eliminate noises from surroundings and power supply.

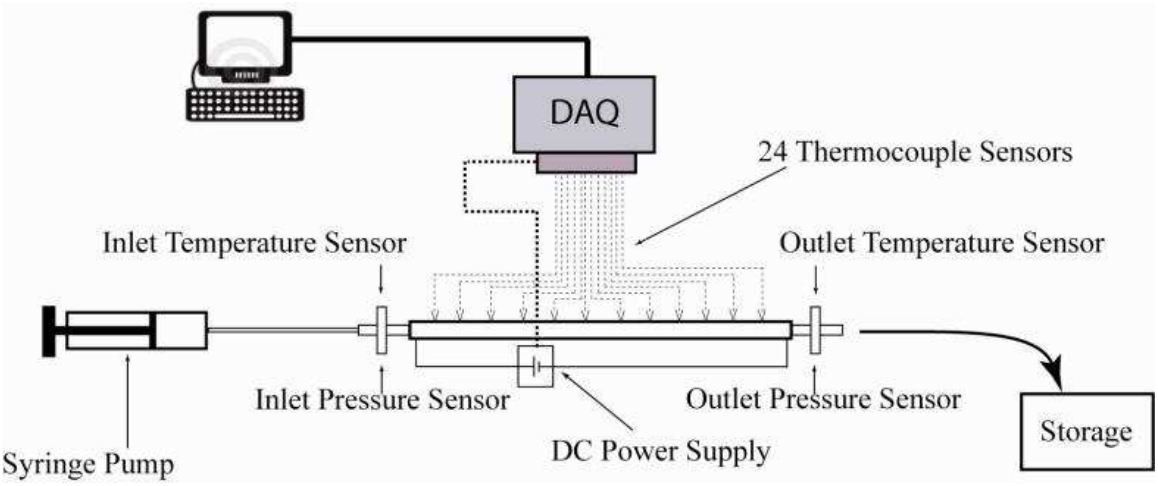

Figure 1. Schematic of experimental setup.

Subcooled fluid was supplied by a constant flow rate syringe pump and collected by the storage tank with a vent to the atmosphere. For flow boiling in the normal boiling regime, the surface temperature was normally a few degrees higher than the saturation temperature. However when CHF was occurring, the surface temperature jumped rapidly and the process was irreversible leading to burnout. During the experiments, input heat flux was increased steadily until the maximum surface temperature of the microchannel reaches the preset value, $150\,^{o}C$ in this work, and the correspondent input power is defined as the critical heat flux in this work. It has been observed when surface temperature reaches to $150\,^{o}C$, the surface temperature rises rapidly and it would be irreversible. When surface temperature reaches to $150\,^{o}C$, the power will be shut down to prevent of damage to the microchannel and measurement system. All thermocouples

and pressure sensors were calibrated before use. The uncertainty of the thermocouples is controlled within 0.5 Kelvin within the whole experimental range, the pressure sensor has an uncertainty of 1.5 % and the average flow rate driven by the syringe pump has an uncertainty of 2%. The system heat loss was measured after the steady-state was achieved in the single phase convection regime just before the boiling occurs. The heat loss is defined as the difference of the input power and the enthalpy increase of the fluids as

$$Q_{HL}\% = \frac{VI - \dot{m}c_p(T_o - T_i)}{VI}100 \quad (2)$$

Such a calculated value represents the maximum possible heat loss. When boiling occurs, the contribution of latent heat transfer will reduce the heat loss. The measured heat loss under typical working conditions was less than 10%.

Due to the small size and easy to be stabilized aqueous alumina nanofluids were used as working fluids. The nanofluids were formulated by the two-step method by dispersing commercial alumina nanoparticles of average particle size of 25 nm into the deionized water, Figure 2.

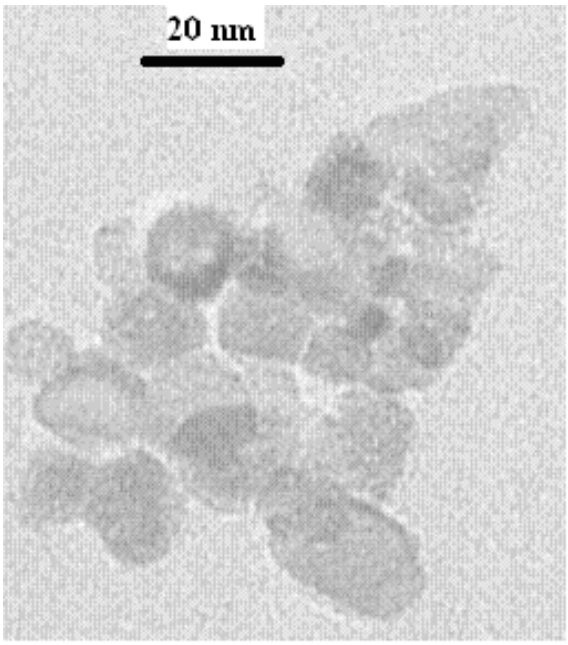

Figure 2. Transmission electron microscopy (TEM) picture of alumina nanoparticles.

An ultrasonic bath was employed to homogenize the alumina nanofluids with three concentrations of 0.001, 0.01, and 0.1 v%. No surfactant or dispersant was added in the formulation process. The relative small particle size and dilute concentrations make the

nanofluids stable sufficiently for the current experimental purpose. Apart from the TEM observation, we also verify the particle dispersion status through a dynamic light scattering (DLS) technique, which measures directly the particle size distribution in a liquid carrier. The DLS results show that the agglomeration of particles is negligible for freshly-made nanofluids.

The working fluid is preheated before inserted into the syringe pump. The syringe also is wrapped up with silicone rubber heater to provide different subcooling. The experiments were conducted under low mass flow rates in the range of 600~1950 kg/m^2s.

6. Results and Discussions

Before conducting nanofluids experiment, a benchmark study using deionized water as the working fluid was conducted. The results showed the CHF value was in the range of 100~350 kW/m^2 and the value of CHF increased with increase of mass flux and initial subcooling. Such results are consistence with experimental investigation of Roday et al (2008) and Hall and Mudawar (2000a) under similar conditions, which shows the validity of the current experimental system. To avoid the surface modification by nanoparticle deposition, which has been observed and suspected to the main reason responsible for high CHF, a number of test sections were constructed in this work. Fresh microchannels were used for each concentration of nanofluids, and the duration of nanofluids usage was kept the same in the comparison. Figure 3 shows SEM pictures of the test section of stainless steel microchannel at the vicinity of the outlet after experiments with (a) boiling water, (b) 0.001 v% alumina, (c) 0.01 v% alumina, and (d) 0.1 v% alumina.

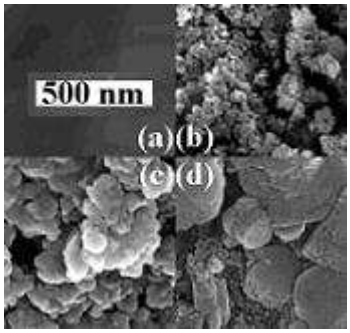

Figure 3. SEM pictures of the test section of stainless steel microchannel close to the outlet after experiments with (a) boiling water, (b) 0.001 v% alumina, (c) 0.01 v% alumina, and (d) 0.1 v% alumina.

The averaged pressure drop across the tube is in the range of 40~140 kPa depending mainly on the flow rate and fluids used. However there is a strong fluctuation in the pressure and pressure drops due to the confined bubbles formed inside the tube. Figure 3 shows an example of inlet and outlet pressure variation for water and 0.01 v% alumina nanofluids when a steady state flow boiling is achieved. For the nanofluids case, both the frequency and amplitude of the inlet pressure fluctuations are larger than those of DI water, which indicated a different bubble activities and flow regimes occurring inside the channel. The critical heat flux is induced with a subsequent increase of heat flux.

Example curves of the variation of subcooled critical heat flux with mass flux and alumina nanofluid concentration (0.001-0.1 v%) are shown in Figures 4 and 5 at two initial subcoolings, which is defined as $\Delta T_{sub,i} = T_{sat} - T_{ins}$ where T_{sat} is the saturated temperature and T_{ins} is the initial working fluid temperature at the inlet, inside the microchannel. The results clearly show that the critical heat flux increased nearly linearly with the increase of mass flux. Both the nanoparticle concentration and initial subcooling affected significantly the value of CHF. CHF increased with particle concentration especially under low mass flux conditions; the increase in CHF with nanofluids concentration appears to be non-linear. The increase in the initial subcooling renders the CHF more difficult to occur. For the given mass flux (600-1700 kg/m^2s) and initial subcooling of $80\,^oC$, the critical heat flux enhancement is within a band of 8% ~ 51%. The maximum CHF enhancement was occurred at the lowest mass flux (651.84 kg/m^2s). For the initial subcooling of $45\,^oC$, the CHF enhancement is around 4% ~ 31% higher than that of deionized water. The critical heat flux enhancement appears to be smaller at the lower initial subcooling. CHF in single microchannels can be increased significantly under very low nanoparticle concentration. The general trends of CHF variation with mass flux and initial subcooling are similar to that of pure fluids in microchannels, and nanofluids in macrochannels.

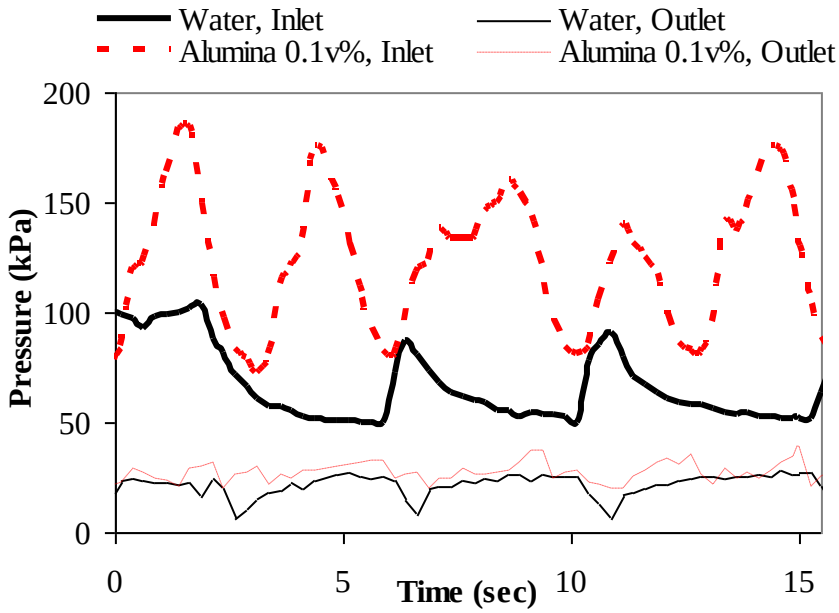

Figure 4. Example inlet and outlet pressure variations for water and 0.01 v% alumina nanofluid inside the microchannel at mass flux of 1630 kg/m^{2}s and heat flux of 200 kW / m^2 .

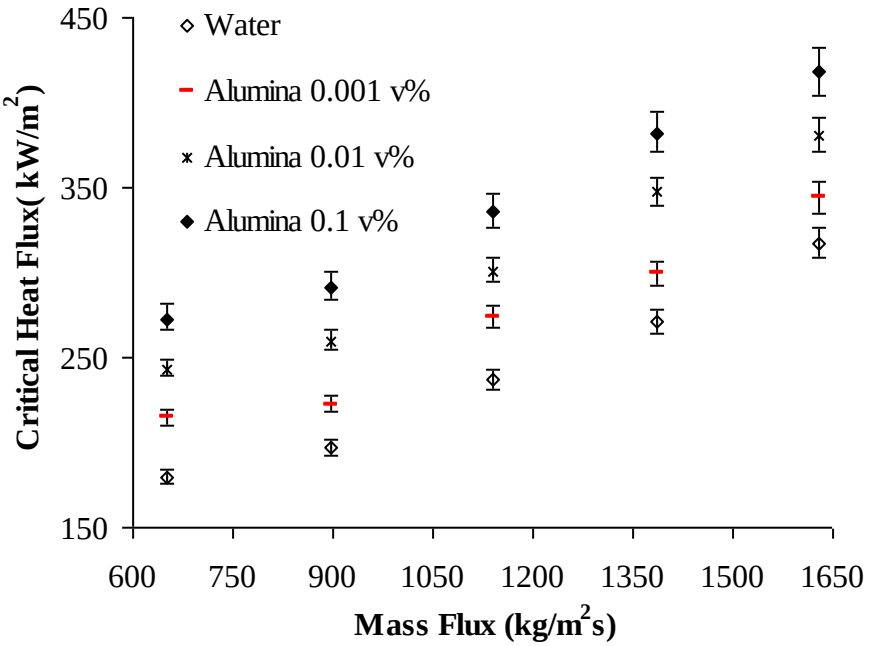

Figure 4. Variation of the critical heat flux with mass flux for deionized water and 0.001-0.1 v% alumina nanofluids (inlet subcooling ~80 ^{o}C).

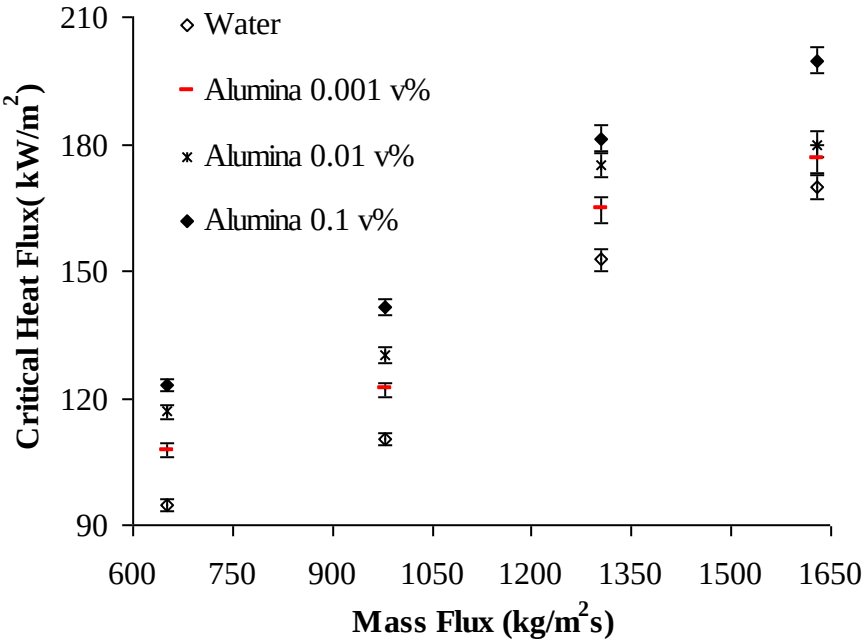

Figure 5. Variation of the critical heat flux with mass flux for deionized water and 0.001-0.1 v% alumina nanofluids (inlet subcooling ~45 ^{o}C).

A few studies have shown that a thin porous layer of nanoparticles would be deposited on heating surface, which would not only change the affinity of working fluid for the substrate, but also would change the spreading of hot spot inside the tube where burnout occurs. The consequences of burnout of heating surface, running with water and nanofluids are consequently different. In large channels, a complete azimuthally failure was occurred for water while a pinhole type failure was observed for nanofluids runs (2008). Figure 6 demonstrate example of burnout of alumina nanofluid inside microchannel. As it can be seen, the thin layer of porous layer of alumina nanoparticles localizes the hot spots and consequently causes a pinhole failure due to burnout.

Figure 6. The tube burnout due to critical heat flux in nanofluid (0.001v% alumina).

Based on the thermodynamic quality of outlet and observation of outlet flow pattern, both data shown in Figures 4 and 5 are in subcooled critical heat flux conditions. The current experimental data were compared with existing CHF correlations for subcooled flow boiling [Lee and Mudawar 2009; Inasaka and Nariai 1987; Vandervort et al 1994; Hall and Mudawar 1999, 2000a,b; Roday and Jensen 2009a]. The best two predictive models, i.e. having lowest mean absolute error, observed are the Hall and Mudawar equation [Hall and Mudawar 2000], as shown in equations (3) and (4) below, and Lee and Mudawar model [Lee and Mudawar 2009], equation (5)

$$q_m = \mathrm{Bo} G h_{fg} \tag{3}$$

$$\mathrm{Bo} = \frac{c_1 \mathrm{We}_d^{c_2} (\rho_f / \rho_g)^{c_3} [1 - c_4 (\rho_f / \rho_g)^{c_5} x_{i,*}]}{1 + 4 c_1 c_4 \mathrm{We}_d^{c_2} (\rho_f / \rho_g)^{c_5 + c_3} (L/d)} \tag{4}$$

where $c_1 = 0.0722, c_2 = -0.312, c_3 = -0.644, c_4 = 0.9, c_5 = 0.724$, $x_{i,*}$ is pseudo-inlet quality, $x_{i,*} = \left(\frac{h_i - h_{f,o}}{h_{fg,o}} \right)$, Bo is boiling number, and Weber number is defined as $\mathrm{We}_d = G^2 d / \sigma \rho_f$.

$$Bo_{Micro} = BoWe_{d_h}^{C} \quad (5)$$

Bo is boiling number defined by Hall and Mudawar correlation [Hall and Mudawar 2000] (see equation 4) and Bo_{Micro} is boiling number of microchannel and $C = 0.121$.

In the evaluation, all thermophysical properties were evaluated at outlet pressure. The Hall and Mudawar model predicted the critical heat flux for water and alumina nanofluids with mean absolute error of 43.2 % and 49.1 % respectively. Using Lee and Mudawar correlation (see equation (5)), the mean absolute error was reduced to 25.1 % and 34.2 % for water and alumina nanofluids respectively. The mean absolute error is defined as

$$M.A.E = \frac{1}{N}\sum \frac{\left|q_{m,\,prediction} - q_{m,measure}\right|}{q_{m,measure}} \quad (6)$$

The nanofluid density can be calculated as $\rho_p\varphi + \rho_f(1-\varphi)$, where φ is the nanoparticle volumetric fraction; ρ_p and ρ_f are the density of nanoparticle material and base liquid. The density of the nanofluid vapor can be calculated as $\rho_g[\rho_p\varphi + \rho_f(1-\varphi)]/[\rho_g\varphi + \rho_f(1-\varphi)]$ [Kim et al 2007; Vafaei and Wen 2011]. The surface tension and enthalpy of alumina nanofluid in low concentrations are nearly same as water [Kim et al 2007].

The Lee and Mudawar model [Lee and Mudawar 2009] is a modified version of the Hall and Mudawar correlation [Hall and Mudawar 2000] aiming for microchannels, the coefficient of Hall and Mudawar correlation [Hall and Mudawar 2000] has been optimized based on a comprehensive data points (5544 data), which might be a reason for a smaller mean absolute error. The Lee and Mudawar model is developed based on current data of water and alumina nanofluids. The sensitivity of coefficient C was firstly assessed, as shown in Figure 7 for alumina nanofluid. The minimum mean absolute error is occurred at $C = 0.2$. Similarly the minimum mean absolute error for water was found to be $C = 0.13$. A modified C value of 0.20 was found to predict CHF of nanofluids pretty well, Figure 8, which reduced the mean absolute error from 34.2% to 30%. $C = 0.13$ was given the best prediction of current deionized water data, which reduced the mean absolute error from 25.1% to 24 %, Figure 9. These figures were also shown that the correlations are slightly lower predicted. Nevertheless, such a predictive accuracy

is acceptable for most of nanofluid applications. Consequently, the modified Lee and Mudawar model equation (5), is recommended for CHF predictions for both water and nanofluids in this work. Different C values can be used to refine the predictions.

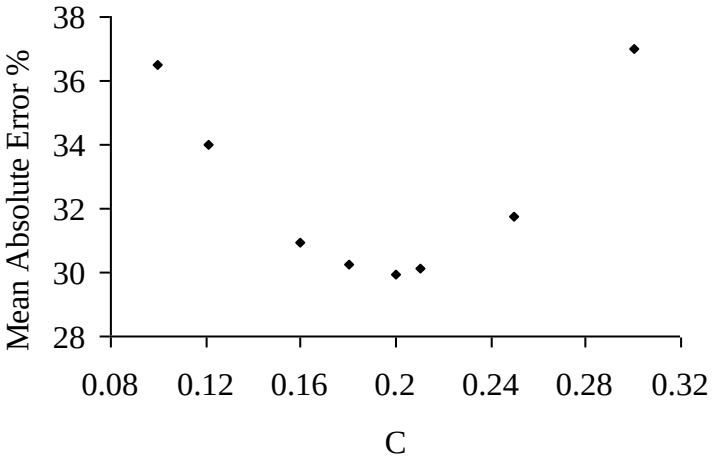

Figure 7. Variation of the mean absolute error with coefficient C of Lee and Mudawar model [Lee and Mudawar 2009] for alumina nanofluids.

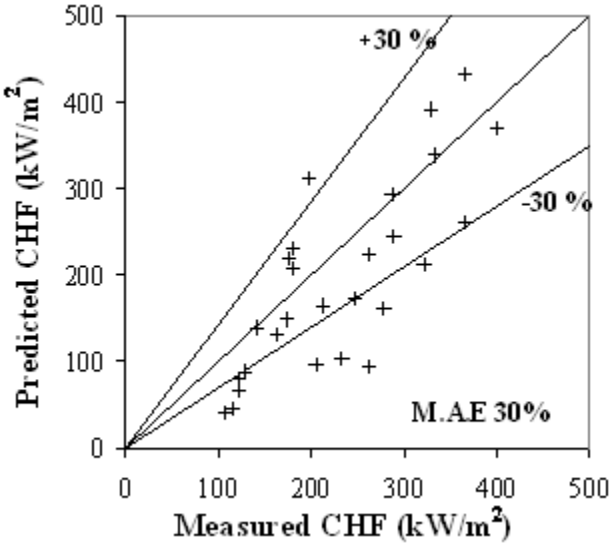

Figure 8. Variation of predicted and measured critical heat flux with 30% error bound for alumina nanofluids, using modification of Lee and Mudawar model (C = 0.2).

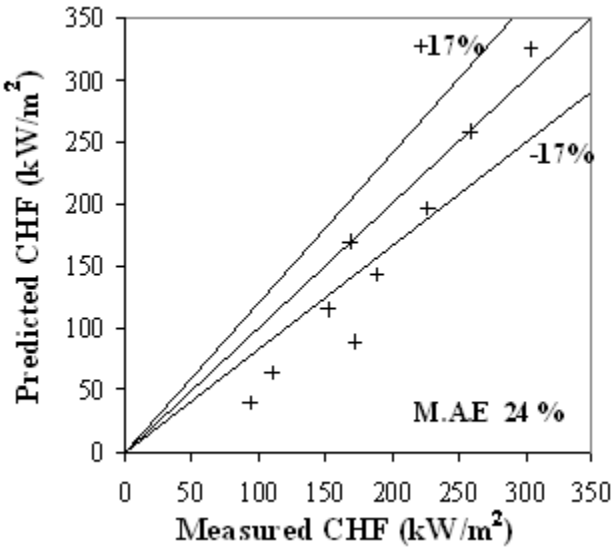

Figure 9. Variation of predicted and measured critical heat flux with 17 % error bound for water, using modification of Lee and Mudawar model (C = 0.13).

7. CONCLUSIONS

An experimental study of CHF phenomenon of water and alumina nanofluids (0.001-0.1 v%) inside single stainless steel microchannels with 45 and 80 ^{o}C subcooling was conducted in this work. The results show that CHF in single microchannels can be increased significantly under very low nanoparticle concentrations. The general trend of CHF variation with mass flux and initial subcooling are similar to that of pure fluids in microchannels and nanofluids in macrochannels, i.e. CHF increase with the increase of mass flux and initial subcoolings. Within all the CHF correlation assessed, the Lee and Mudawar model [Lee and Mudawar 2009] was found to give the best prediction with a mean absolute error of 34% for nanofluids data. With further refinement of its coefficient value, the mean absolute errors of predictive CHF were 24 % and 30 % for deionized water and alumina nanofluid respectively.

Acknowledgement: The authors would like to extend their thanks to EPSRC for financial support under Grant No: EP/E065449/1.

Nomenclature

Bo Boiling number

C_i (i=1:5) Constant in the correlation

c_p Specific heat

d	Diameter
G	Mass flow rate
h	Enthalpy of fluid
h_f	Enthalpy of saturated fluid
h_g	Enthalpy of saturated vapor
h_{fg}	Latent heat of vaporization
I	Current
L	Length
$\dot{m}$	Mass flow rate
q_m	Critical heat flux
Q_{HL}	Heat loss power
T	Temperature
V	Voltage
We	Weber number
$x_{i,*}$	Pseudo-inlet quality

Greek Symbols

ρ	Density
σ	Surface tension

Subscribes

f	Saturated liquid
g	Saturated vapor
h	Hydraulic
i	Inlet
ins	Initial
Micro	Microchannel
o	Outlet
sub	Subcooled
sat	Saturated

Table 1. Literature review on CHF experiments in minichannels and microchannels.

Reference	**Channel Geometry, working fluids and operational conditions**	**Main results and remarks**
Park and Thome (2010)	**Materials :** Copper multichannels **Geometry** 20 parallel channels 467×4052 μm 29 parallel channels 199×756 μm $L(mm) = 20$ **Conditions:** $G(kg/m^2s) =$ 100-4000 $\Delta T_{sub}(^oC) =$ 0-24 **Working fluid:** R-134a, R-236fa, R-245fa	• CHF increased with mass flux while the rate of increase was slower at higher mass fluxes. • CHF increased moderately with increasing inlet subcooling. • The inlet subcooling played a weaker role, as the channel size decreased.
Lee and Mudawar (2009)	**Materials :** Copper multichannels **Geometry :** $d_h(\mu m) = 175.7, 200, 334.1, 415.9$ **Conditions:** $T_i(C) =$ -30 to 20 $G(kg/m^2s) =$ 672-2013 **Working fluid:** HFE 7100	• Subcooled CHF was triggered by vapor blanket formation along the micro-channel walls despite the presence of abundant core liquid. • CHF heat flux increased with increasing mass velocity and subcooling. • CHF increased with decreasing hydraulic diameter for a given total mass flow rate because of increased mass velocity. • A high subcooling reduced both bubble departure diameter and void fraction, and practically prevented the flow pattern transitions beyond the bubbly regime.
Roday and Jensen (2009c)	**Materials :** Stainless steel tubes **Geometry :** $d(mm) =$ 0.286, 0.43, 0.7 $L(mm) =$ 17.26 - 96 **Conditions:** $\Delta T_{sub}(^oC) =$ 2 - 80 $G(kg/m^2s) =$ 315 - 1570 **Working fluid:** Deionized water, R-123	• CHF decreased with increasing of heated length, at a fixed value of inlet subcooling or exit quality. • For a fixed value of inlet subcooling, CHF increased as the exit pressure increased. . • CHF increased substantially with reduction of tube diameter from 0.427 to 0.286 mm. • The difference of CHF for tube diameters of 0.427 mm and 0.700 mm was not substantial.
Roday et al (2008) & Rody and Jensen (2009b)	**Materials :** Stainless steel tubes **Geometry:** $d(mm) =$ 0.286, 0.427, 0.7 $L(mm) = 59$ **Conditions:**	• CHF increased with increasing of mass flux. • For 0.286 mm and 0.7 mm tubes, the CHF decreased with increasing of heated length. • For mass flux of 320 kg/m^2s, $L/d \approx 140$, and exit pressure close to atmospheric, CHF increased substantially

	$\Delta T_{sub}(^{o}C) = 2\text{-}50$ $G(kg/m^2s) = 315\text{-}1570$ **Working fluid:** Deionized water	with reduction of tube diameter from 0.427 mm to 0.286 mm, while the difference of CHF was not much for tubes of 0.427 mm and 0.7 mm. • CHF increased as exit pressure increased. • At higher inlet subcooling, CHF slightly decreased as inlet subcooling decreased, but at lower inlet subcoolings, the critical heat flux increased with decreasing of subcooling. • CHF first decreased with increasing of exit quality in subcooled region, but with further increase in quality (near zero quality and above), CHF is found to have an increasing trend with quality.
Agostini et al (2008)	**Materials :** Silicon multichannel **Geometry :** 67 parallel channels $223 \times 680\ \mu m$ $L(mm) = 20$ **Conditions:** $G(kg/m^2s) = 276\text{-}992$ $\Delta T_{sub}(^{o}C) = 0.4 - 15.3$ **Working fluid:** R-236fa	• The inlet subcoolings ($0.4 \le \Delta T_{sub,i} \le 15.3^{o}C$) have a negligible influence on the saturated CHF. • CHF increased with mass flux.
Kuan and Kandlikar (2008)	**Materials:** Copper multichannel **Geometry :** 6 parallel $1054 \times 157\ \mu m$ channels **Conditions:** $G(kg/m^2s) = 50.4\text{-}231.7$ $T_i(C) = 25$ **Working fluid:** Water, R-123	• Flow restrictors were used at the inlet of each microchannel to avoid the reverse flow phenomenon and stabilize the flow boiling process. • CHF was found to increase with increasing Weber number, i.e, CHF increased with mass flux.
Kuo and Peles (2008)	**Materials :** Silicon based multichannel **Geometry :** 5 parallel $200 \times 253\ \mu m$ channels $L(mm) = 10$ **Conditions:** $G(kg/m^2s) = 86\text{-}303$ **Working fluid:** Water	• Dryout is the mechanism of triggering CHF for flow boiling of water in microchannels at sub-atmospheric pressure, at low to moderate mass fluxes. • The boiling number at the critical heat flux condition is approximately a constant. • CHF is not strongly dependent on system pressure.
Kosar and Peles (2007) & Kosar et al (2005)	**Materials :** Silicon based multichannels **Size:** 5 Parallel $200 \times 264\ \mu m$ Channel	• CHF increased linearly with mass flux and decreased with exit quality. • The exit mass quality at the critical heat flux condition decreased with increasing mass

	$L(mm) = 10$ **Conditions:** $G(kg/m^2s) = 291\text{-}1118$ **Working fluid:** R-123, Water	velocity at the fixed pressure. • CHF was triggered at relatively high qualities during annular flow, which was confirmed by visualization of flow patterns, and relatively high exit quality at the critical heat flux conditions. • As exit pressure increased, CHF increased first to a maximum value and then declined.
Qi et al (2007a,b)	**Materials :** Stainless steel Microtube **Geometry :** $d(mm) = 0.531, 0.834, 1.042, 1.931$ **Conditions:** $G(kg/m^2s) = 700\text{-}3000$ **Working fluid:** Nitrogen	• For given mass flux, the critical heat flux increased gradually with decreasing of tube diameter. • For all given tubes, CHF increased with increasing of mass flux, whereas a reverse trend was observed for the critical mass quality.
Wojtan et al (2006)	**Materials :** Stainless steel tubes **Geometry :** $d(mm) = 0.5, 0.8$ $L(mm) = 20\text{-}70$ **Conditions:** $\Delta T_{sub}(^oC) = 2\text{-}15$ $G(kg/m^2s) = 400\text{-}1600$ We_L=293-21044 **Working fluid:** R-134a, R-245fa	• The highest CHF occurred for the shortest heated length. • CHF increased with increasing of mass flux. • CHF inside 0.8 mm microchannel was higher than that of 0.5 mm one; the difference became larger as the mass velocity increased. • No significant influence of subcooling in range of 2-15 ^oC was observed on CHF. • CHF was higher for R-245fa compared to R-134a, while heated length was bigger than 20 mm.
Qu and Mudawar (2004)	**Materials:** Copper multichannel **Geometry :** 21 parallel 215×821 μm channels **Conditions:** $G(kg/m^2s) = 86\text{-}368$ $T_i(C) = 30, 60$ **Working fluid:** Deionized water	• CHF increased with increasing mass flux. • Because of loss of subcooling due to the backward vapor flow and re-mixing, the CHF was independent of the inlet temperature.
Mudawar and Bowers (1999)	**Materials :** Stainless steel tubes **Geometry:** $d(mm) = 0.406\text{-}2.54$ $L(mm) = 5.6$ **Conditions:** $G(kg/m^2s) = 5000\text{-}134000$	• CHF increased with increasing mass flux, decreasing of tube diameter, and decreasing of ratio of the heated length to diameter. • CHF increased fairly linear with increasing of subcooling.

	$T_i(C) = 18\text{-}70$ **Working fluid:** Water	
Vandervort et al (1994)	**Materials :** Stainless steel 304 & 316, nickel, brass and inconel tube **Geometry:** $d(mm) = 0.3\text{-}2.7$ $L/d = 0.2\text{-}50$ **Conditions:** $G(kg/m^2s) = 5000\text{-}40000$ $\Delta T_{sub,o}(^oC) = 40\text{-}135$ **Working fluid:** Water	• CHF increased as mass flux and subcooling increased, and decreased with of increasing of tube size. • CHF decreased as the length/diameter ratio increased, especially while length/diameter ratio was smaller than 10. • CHF decreased slightly with increasing of exit pressure. • No significant changes were observed in CHF over the range of dissolved gas concentration from zero to saturated level. • No significant changes were observed in CHF with variation of tube materials.
Bowers and Mudawar (1994)	**Materials:** Oxygen-free copper multichannel **Geometry :** $d(mm) = 0.510, 2.54$ $L/d = 3.94, 19.6$ **Conditions:** V_L(ml/min)=up to 95 $\Delta T_{sub,i}(^oC) = 10\text{-}32$ **Working fluid:** R-133	• CHF was not function of inlet subcooling at low flaw rates. • CHF was triggered at upstream of the exit. • CHF of microchannels was higher than that inside mini-channels.
Inasaka and Nariai (1987)	**Materials :** Stainless steel tubes **Geometry :** $d(mm) = 1\text{-}3$ $L(mm) = 10\text{-}100$ **Conditions:** $G(kg/m^2s) = 7000\text{-}20000$ **Working fluid:** water	• For a given mass flux, CHF increased inside narrow tubes.

References

Agostini B., Revellin R., Thome J. R., Fabbri M., Michel B., Calmi D., Kloter U.,2008, High heat flux flow boiling in silicon multi-microchannels-Part III: Saturated critical heat flux of R236fa and two-phase pressure drops, International Journal of Heat and Mass Transfer 51, 5426-5442.

Bowers M. B., Mudawar I., 1994, High flux boiling in low flow rate, low pressure drop mini-channel and micro-channel heat sinks, International Journal of Heat and Mass Transfer 37, 321-332.

Bang I. C., Chang S. H.,2005, Boiling heat transfer performance and phenomena of Al2O3–water nano-fluids from a plain surface in a pool, International Journal of Heat and Mass Transfer 48, 2407-2419.

Buongiorno J et al, 2009, A benchmark study on the thermal conductivity of nanofluids, Journal of Applied Physics 106, 094312.

Celata G. P., Cumo M., Mariani A., 1993, Burnout in highly subcooled water flow boiling in small diameter tubes, International Journal of Heat and Mass Transfer 36, 1269-1285.

Celata G. P., Cumo M., Mariani A., 1994, Assessment of correlations and models for the prediction of CHF in water subcooled flow boiling, International Journal of Heat and Mass Transfer 37, 237–255.

Doroshckuk V. E., Levitan L. L., Lantzman F. P., 1975, Investigation into burnout in uniformly heated tubes, ASME Paper, 75-WA/HT-22.

Forrest E.,Williamson E., Buongiorno J., Hu L. W., Rubner M., Cohen R., 2010, Augmentation of nucleate boiling heat transfer and critical heat flux using nanoparticle thin-film coatings, International Journal of Heat and Mass Transfer 53, 58-67.

Gerardi C., Buongiorno J., Hu L. W., McKrell T., 2010, Study of bubble growth in water pool boiling through synchronized, infrared thermometry and high-speed video, International Journal of Heat Mass Transfer 53, 4185-4192.

Haramura Y., Katto Y., 1983, A new hydrodynamic model of CHF applicable widely to both pool and forced convection boiling on submerged bodies in saturated liquids. International Journal of Heat and Mass Transfer 26, 389-399.

Hall D., Mudawar I., 1999, Ultra-high critical heat flux (CHF) for subcooled water flow boiling-II: high-CHF database and design equations, International Journal of Heat and Mass Transfer 42, 1429-1456.

[a]Hall D., Mudawar I., 2000, Critical heat flux (CHF) for water flow in tubes-II, Subcooled CHF correlations, International Journal of Heat and Mass Transfer 43, 2605-2640.

[b]Hall D., Mudawar I., 2000, Critical heat flux (CHF) for water flow in tubes-I, Compilation and assessment of world CHF data, International Journal of Heat and Mass Transfer 43, 2573-2604.

Inasaka F., Nariai H., 1987, Critical heat flux and flow characteristics of subcooled flow boiling in narrow tubes, JSME International Journal 30, 1595-1600.

Katto Y., 1978, A generalized correlation of critical heat flux for the forced convection boiling in vertical uniformly heated round tubes. International Journal of Heat and Mass Transfer 21, 1527-1542.

Katto Y., Ohno H., 1984, An improved version of the generalized correlation of critical heat flux for the forced convective boiling in uniformly heated vertical tubes, International Journal of Heat and Mass Transfer 27, 1641-1648.

Kandlikar S. G., 2001, A theoretical model to predict pool boiling CHF incorporating effects of contact angle and orientation, Journal of Heat Transfer 123, 1071-1079.

Kandlikar S. G., Steinke M. E., 2002, Contact angles and interface behavior during rapid evaporation of liquid on a heated surface, International Journal of Heat and Mass Transfer 45, 3771-3780.

Kosar A., Kuo C. J., Peles Y., 2005, Boiling heat transfer in rectangular microchannels with reentrant cavities, International Journal of Heat and Mass Transfer 48, 4867-4886.

[a]Kim S. J., Bang I. C., Buongiorno J., Hu L. W., 2007, Study of pool boiling and critical heat flux enhancement in nanofluids, Bulletin of the Polish Academy of Sciences, Technical Sciences 55, 211-216.

[b]Kim S. J., Bang I. C., Buongiorno J., Hu L. W., 2007, Surface wettability change during pool boiling of nanofluids and its effect on critical heat flux, International Journal of Heat and Mass Transfer 50, 4105-4116.

[c]Kim S. J., Bang I. C., Buongiorno J., Hu L. W., 2007, Surface wettability change during pool boiling of nanofluids and its effect on critical heat flux, International Journal of Heat and Mass Transfer 50, 4105-4116.

Kosar A., Peles Y., 2007, Critical heat flux of R-123 in silicon-based microchannels, ASME Journal of Heat Transfer 129, 844-851.

Kim S. J., Buongiorno J., Hu L. W.,2008, Alumina nanoparticles enhance the flow boiling critical heat flux of water at low pressure, Journal Heat Transfer 130, 044501-3.

Kuan W. K., Kandlikar S. G., 2008, Experimental study and model on critical heat flux of refrigerant-123 and water in microchannels, Journal of Heat Transfer 130, 0345031-5.

Kuo C. J., Peles Y., 2008, Critical heat flux of water at sub atmospheric pressures in microchannels, Journal of Heat Transfer 130, 0724031-7.

Kim S. J., McKrell T., Buongiorno J., Hu L. W., 2009, Experimental study of flow critical heat flux in alumina-water, zinc-oxide-water, and diamond-water nanofluids, Journal of Heat Transfer 131,0432041-0432045.

Lazarek G. M., Black S. H., 1982, Evaporative heat transfer, pressure drop and critical heat flux in a small vertical tube with R-113, International Journal of Heat and Mass Transfer 25, 945-960.

Lee J., Mudawar I., 2009, Critical heat flux for subcooled flow boiling in micro-channel heat sinks, International Journal of Heat and Mass Transfer 52, 3341-3352.

Mudawar I., Bowers M. B., 1999, Ultra-high critical heat flux (CHF) for subcooled water flow boiling-I: CHF data and parametric effects for small diameter tubes, International Journal of Heat and Mass Transfer 42, 1405-1428.

Mukherjee A., Kandlikar S. G., 2007, Numerical study of single bubbles with dynamics contact angle during nucleate pool boiling, International Journal of Heat and Mass Transfer 50, 127-138.

Park J. E., Thome J. R., 2010, Critical heat flux in multi-microchannel copper elements with low pressure refrigerants, International Journal of Heat and Mass Transfer 53, 110-122.

Qu W., Mudawar I., 2004, Measurement and correlation of critical heat flux in two-phase micro-channel heat sinks, International Journal of Heat and Mass Transfer 47, 2045-2059.

[a]Qi S. L., Zhang P., Wang R. Z., Xu L. X., 2007, Flow boiling of liquid nitrogen in micro-tubes: Part II-Heat transfer characteristics and critical heat flux, International Journal of Heat and Mass Transfer 50, 5017-5030.

[b]Qi S. L., Zhang P., Wang R. Z., Xu L. X., 2007, Flow boiling of liquid nitrogen in micro-tubes: Part I - The onset of nucleate boiling, two-phase flow instability and two-phase flow pressure drop, International Journal of Heat and Mass Transfer 50, 4999-5016.

Roday A. P., Borca-Tasçiuc T., Jensen M. K., 2008, The critical heat flux condition with water in a uniformly heated microtube, ASME Journal of Heat Transfer 130, 0129011-01290110.

Revellin R., Thome J. R., 2008, A theoretical model for the prediction of the critical heat flux in heated microchannels, International Journal of Heat and Mass Transfer 51, 1216-1225.

[a]Roday A. P., Jensen M. K., 2009, Study of the critical heat flux condition with water and R-123 during flow boiling in microtubes, Part II - Comparison of data with correlations and establishment of a new subcooled CHF correlation, International Journal of Heat and Mass Transfer 52, 3250-3256

[b]Roday A. P., Jensen M. K., 2009, A review of the critical heat flux condition in mini-and microchannels, Journal of Mechanical Science and Technology 23, 2529-2547.

[c]Roday A. P., Jensen M. K. ,2009, Study of the critical heat flux condition with water and R-123 during flow boiling in microtubes, Part I: Experimental results and discussion of parametric effects, International Journal of Heat and Mass Transfer 52, 3235-3249.

Rea U., McKrell T., Hu L. W., Buongiorno J., 2009, Laminar convective heat transfer and viscous pressure loss of alumina-water and zirconia-water nanofluids, International Journal of Heat and Mass Transfer 52, 2042-2048.

Tong L. S., 1968, Boundary-layer analysis of the flow boiling crisis, International Journal of Heat and Mass Transfer 11, 1208-1211.

Theofanous T. G., Dinh T. N., 2006, High heat flux boiling and burnout as microphysical phenomena: mounting evidence and opportunities, Multiphase Science and Technology 18, 1-26.

Vandervort C. L., Bergles A. E., Jensen M. K., 1994, An experimental study of critical heat flux in very high heat flux subcooled boiling, International Journal of Heat and Mass Transfer 37, 161-173.

Vafaei S., Podowski M. Z., 2004, The modeling of liquid droplet shape on horizontal and inclined surfaces, 5th ICMF, Yokohama, Japan, May 30-June 4.

Vafaei S., Podowski M. Z., 2005, Analysis of the relationship between liquid droplet size and contact angle, Advances in Colloid and Interface Science 113, 133-146.

Vafaei S., Borca-Tasciuc T., Podowski M. Z., Purkayastha A., Ramanath G., Ajayan P. M., 2006, Effect of nanoparticles on sessile droplet contact angle, Nanotechnology 17, 2523-2527.

Vafaei S., Purkayastha A., Jain A., Ramanath G., Borca-Tasciuc T., 2009, Effect of nanoparticles on the liquid-gas surface tension of Bi_2Te_3 nanofluids, Nanotechnology 20, 185702-185708.

Vafaei S., Borca-Tasciuc T., Wen D., 2010, Theoretical and experimental investigation of quasi-steady-state bubble growth on top of submerged stainless steel nozzles, Colloids and Surfaces A: Physicochemical and Engineering Aspects 369, 11-19.

Vafaei S., Borca-Tasciuc T., Wen D., 2010, Theoretical and experimental investigation of quasi-steady-state bubble growth on top of submerged stainless steel nozzles, Colloids and Surfaces A: Physicochemical and Engineering Aspects 369, 11-19.

[a]Vafaei S., Wen D., 2010, Critical heat flux (CHF) of subcooled flow boiling of alumina nanofluids in a horizontal microchannel, ASME Journal of Heat Transfer 132, 1024041-7

[b]Vafaei S., Wen D., 2010, The effect of gold nanoparticles on the dynamics of gas bubbles, Langmuir 26, 6902-6907.

[c]Vafaei S., Wen D., 2010, Bubble formation in a quiescent pool of gold nanoparticle suspension, Advances in Colloid and Interface Science 159, 72-93.

[d]Vafaei S., Wen D., 2010, The effect of gold nanoparticles on the spreading of triple line. Microfluidics and Nanofluidics 8, 843-848.

[e]Vafaei S., Wen D., 2010, Bubble formation on a submerged micronozzle, Journal of Colloid and Interface Science 343, 291-297.

Vafaei S., Wen D., Borca-Tasciuc T., 2011, Nanofluids surface wettability through asymptotic contact angle, Langmuir 27, 2211-2218.

Vafaei S., Angeli P., Wen D., 2011, Bubble growth rate from stainless steel substrate and needle nozzles, Colloids and Surfaces A: Physicochemical and Engineering Aspects 387, 240-247.

[a]Vafaei S., Wen D., 2011, Spreading of triple line and dynamics of bubble growth inside nanoparticle dispersions on top of a substrate plate, Journal Colloid Interface Science 362, 285-291.

[b]Vafaei S., Wen D., 2011, Convective heat transfer of aqueous alumina nanosuspensions in a horizontal mini-channel. Heat and Mass Transfer 48, 349-357.

Wen D., Ding Y., 2004, Experimental investigation into convective heat transfer of nanofluids at the entrance region under laminar flow conditions, International Journal of Heat and Mass Transfer 47, 5181-5188.

Wojtan L., Revellin R., Thome J. R., 2006, Investigation of saturated critical heat flux in a single, uniformly heated microchannel, Experimental Thermal and Fluid Science 30, 765-774.

[a]Wen, D., 2008, On the role of structural disjoining pressure to boiling heat transfer with thermal nanofluids, Journal of Nanoparticle Research 10, 1129-1140

[b]Wen, D., 2008, Mechanisms of thermal nanofluids on enhanced critical heat flux (CHF), International Journal of Heat and Mass Transfer 51,4958-4965

Wen D., Lin G., Vafaei S., Zhang K., 2009, Review of nanofluids for heat transfer applications, Journal of Partriology, 7, 141-150.

Zhang W., Hibiki T., Mishima K., Mi Y., 2006, Correlation of critical heat flux for flow boiling of water in mini-channels, International Journal of Heat and Mass Transfer 49, 1058-1072.